Eur J Nucl Med Mol Imaging (2013) 40:580–593
DOI 10.1007/s00259-012-2322-6

ORIGINAL ARTICLE

Low background and high contrast PET imaging of amyloid-β with [^{11}C]AZD2995 and [^{11}C]AZD2184 in Alzheimer's disease patients

Anton Forsberg · Anders Juréus · Zsolt Cselényi · Maria Eriksdotter · Yvonne Freund-Levi · Fredrik Jeppsson · Britt-Marie Swahn · Johan Sandell · Per Julin · Magnus Schou · Jan Andersson · Peter Johnström · Katarina Varnäs · Christer Halldin · Lars Farde · Samuel Svensson

Received: 23 August 2012 / Accepted: 10 December 2012 / Published online: 17 January 2013

Abstract
Purpose The aim of this study was to evaluate AZD2995 side by side with AZD2184 as novel PET radioligands for imaging of amyloid-β in Alzheimer's disease (AD).

Methods In vitro binding of tritium-labelled AZD2995 and AZD2184 was studied and compared with that of the established amyloid-β PET radioligand PIB. Subsequently, a first-in-human in vivo PET study was performed using [^{11}C]AZD2995 and [^{11}C]AZD2184 in three healthy control subjects and seven AD patients.

Results AZD2995, AZD2184 and PIB were found to share the same binding site to amyloid-β. [^{3}H]AZD2995 had the highest signal-to-background ratio in brain tissue from patients with AD as well as in transgenic mice. However, [^{11}C]AZD2184 had superior imaging properties in PET, as shown by larger effect sizes comparing binding potential values in cortical regions of AD patients and healthy controls. Nevertheless, probably due to a lower amount of nonspecific binding, the group separation of the distribution volume ratio values of [^{11}C]AZD2995 was greater in areas with lower amyloid-β load, e.g. the hippocampus.

Conclusion Both AZD2995 and AZD2184 detect amyloid-β with high affinity and specificity and also display a lower degree of nonspecific binding than that reported for PIB. Overall [^{11}C]AZD2184 seems to be an amyloid-β radioligand with higher uptake and better group separation when compared to [^{11}C]AZD2995. However, the very low nonspecific binding of [^{11}C]AZD2995 makes this radioligand potentially interesting as a tool to study minute levels of amyloid-β. This sensitivity may be important in investigating, for example, early prodromal stages of AD or in the longitudinal study of a disease modifying therapy.

Keywords Alzheimer's disease · Amyloid-β imaging · [^{11}C]AZD2995 · [^{11}C]AZD2184 · PET imaging

Electronic supplementary material The online version of this article (doi:10.1007/s00259-012-2322-6) contains supplementary material, which is available to authorized users.

A. Juréus · F. Jeppsson · B.-M. Swahn · J. Sandell · P. Julin · S. Svensson
Neuroscience Research & Therapy Area, AstraZeneca Research & Development, Södertälje, Sweden

A. Forsberg (✉) · Z. Cselényi · M. Schou · J. Andersson · P. Johnström · K. Varnäs · C. Halldin · L. Farde
Centre for Psychiatry Research, Department of Clinical Neuroscience, Karolinska Institutet, Stockholm, Sweden
e-mail: anton.forsberg@ki.se

Z. Cselényi · M. Schou · P. Johnström · L. Farde
AstraZeneca Translational Sciences Centre, PET CoE, Department of Clinical Neuroscience, Karolinska Institutet, Karolinska Hospital, Stockholm, Sweden

M. Eriksdotter · Y. Freund-Levi
Clinical Geriatrics, Department of Neurobiology, Care Sciences and Society, Karolinska Institutet, Stockholm, Sweden

M. Eriksdotter · Y. Freund-Levi
Department of Geriatric Medicine, Karolinska University Hospital, Stockholm, Sweden

F. Jeppsson
Science for Life Laboratory, Division of Translational Medicine and Chemical Biology, Department of Medical Biochemistry and Biophysics, Karolinska Institutet, Stockholm, Sweden

Introduction

Deposition of amyloid plaques containing Aβ fibrils in the brain is a key biomarker for the post mortem diagnosis of Alzheimer's disease (AD) [1, 2]. Using PET it is possible to study amyloid-β pathology in vivo using radioligands that specifically target amyloid-β. The first and so far most widely applied radioligand is [^{11}C]PIB (2-[4′-(methylamino)phenyl]-6-hydroxybenzothiazole), which binds specifically to amyloid-β plaques [3]. PET imaging with [^{11}C]PIB has been demonstrated to be able to distinguish between AD patients and healthy controls with high specificity and sensitivity [4, 5]. However, the observation that [^{11}C]PIB displays relatively high nonspecific binding in nontarget areas may pose a limitation to its ability to measure discrete changes in amyloid-β load caused by disease progression or drug therapy that lowers amyloid-β. PET imaging studies using [^{11}C]PIB have also exposed limitations when it is used in mouse models of amyloidosis possibly due to a lower number of binding sites than in AD patients [6, 7].

[^{18}F]FDDNP (2-(1-{6-[18]fluoroethyl}(methyl)amino)-2-naphthyl)ethylidene)malononononitrile) binds both amyloid-β plaques and neurofibrillary tangles, and it has therefore been suggested that it could be sensitive to pathological changes early in the disease progress [8]. However, when compared to other amyloid radioligands, [^{18}F]FDDNP has a ninefold lower specific binding signal in AD patients, which might explain why recent longitudinal studies have shown different results [9]. One study has shown a relationship between [^{18}F]FDDNP and memory decline [10] while another study using [^{18}F]FDDNP failed to reveal pathological progression [11]. Thus, a PET radioligand with lower nonspecific and higher specific binding to amyloid-β would provide an improvement in in vivo PET imaging in human subjects and in various animal models of AD.

The aim of the present study was to develop a ^{11}C-labelled ligand with minimal nonspecific binding for research and multitracer studies. The overall hypothesis was that lower lipophilicity (logD) than that of previously developed radioligands would translate into lower nonspecific binding. Data have previously been presented for [^{11}C]AZD2184 [12–14] and [^{18}F]AZD4694 [15, 16]. In parallel a third compound, AZD2995 with an even lower logD (1.3) than that of AZD2184 (1.8) and PIB (2.8) [17] has been developed.

The first aim of this study was to examine the binding properties of AZD2995 in a preclinical setting and compare these properties with those of AZD2184 and PIB. In addition, binding was examined in an initial PET study of [^{11}C]AZD2995 in control subjects and AD patients. The previously developed radioligand [^{11}C]AZD2184 was used in parallel for comparative purposes.

Material and methods

Preclinical studies

Experimental animals

Transgenic mice (approximately 18 months old) were used for in vitro binding assays and to examine labelling after in vivo administration of the respective radioligand as described below. Double transgenic APP/PS1 mice were generated in-house via heterozygous breeding of mice expressing the 695 isoform of the human AD amyloid precursor protein containing the double mutation Lys670-Asn,Met671-Leu (Swedish mutation) [18] under transcriptional control of the hamster prion promoter and of mice expressing mutated human presenilin gene Met146-Leu under transcriptional control of the rat platelet-derived growth factor-b promoter [19]. All animals were housed at the AstraZeneca animal facility (AstraZeneca R&D, Södertälje, Sweden). Housing was humidity- and temperature-controlled. Food and water were provided ad libitum and the light/dark cycle was 12/12 h. All animal studies were approved by the Stockholm Animal Research Ethics Committee, and all experiments were performed in accordance with the guidelines of the Swedish Animal Welfare Agency.

Human tissue

Cortical samples from AD patients were acquired from the Netherlands Brain Bank and used to examine radioligand binding to amyloid-β plaques. The tissue samples were used in accordance with the Swedish Biobank Law and AstraZeneca guidelines to protect the integrity of the donor. Cortical samples were from the brain of a female 83-year-old ApoE 4/4 carrier with diagnosed AD (from the gyrus inferior frontalis).

Radioligand binding and competition assays

The saturation binding assays on synthetic human Aβ(1-40) fibrils to determine the equilibrium dissociation constant (K_d) and density of binding sites (B_{max}) of [^{3}H]AZD2995 have been previously described [15]. To further characterize the binding mode of AZD2995, competition binding studies with unlabelled compound were conducted using either Aβ(1-40) or Aβ(1-42) fibrils at different concentrations of [^{3}H]PIB (0.5–35 nM) as described previously [15]. All measurements were performed in duplicate and repeated three to six times. The K_d, B_{max} and pIC_{50} were determined from the experimental results by nonlinear regression analysis using GraphPad Prism (version 4.03; GraphPad Software, San Diego, CA).

Dissociation assay

Dissociation studies were used to determine the dissociation rates and reversibility of [^{3}H]AZD2995 binding to synthetic Aβ(1-40) fibrils. For this purpose, 400 μl of 0.25 μM Aβ (1-40) in phosphate buffer (pH 7.5) and 50 μl of 10 nM [^{3}H] AZD2995 were dissolved in assay buffer with 0.1 % BSA and incubated for 2.5 h in ABgene Mark II 96 deep-well plates. The displacement was initiated by addition of 10 μl of 460 μM AZD2995 in DMSO at different time points (0–90 min) prior to filtration. Additions of 10 μl DMSO were done to control wells at the time points 90, 60 and 30 min prior to filtration to control for the dissociation effect of the DMSO. The displacement was terminated by filtration through a Whatman GF/B glass microfibre filter (Whatman International, Maidstone, UK) prewetted with 0.5 % BSA in wash buffer, with a Brandel M-48TI cell harvester (Brandel, Gaithersburg, MD) and washed rapidly three times with 2 ml of ice-cold wash buffer (10 mM HEPES, pH 7.4, containing 500 mM NaCl). The filters were equilibrated for 2 h with 4 ml of Ultima Gold scintillation fluid (PerkinElmer, Waltham, MA) and counted in a Packard Tricarb 2900TR liquid scintillation analyser (PerkinElmer). Results were corrected for nonspecific, nondisplaceable binding, defined as the number of counts from wells without Aβ(1-40) fibrils using only assay buffer. All measurements were performed in duplicate and each experiment was repeated four times.

In vitro autoradiography on brain sections from APP/PS1 mice and AD patient

In vitro autoradiography was performed as described previously [13, 15]. Briefly, 10 μm thick cryo-cut tissue sections from APP/PS1 transgenic mice or human post mortem AD brain were incubated in 50 mM Tris buffer (pH 7.4) at room temperature followed by 30 min incubation with [^{3}H]PIB, [^{3}H]AZD2184 or [^{3}H]AZD2995 in Tris buffer.

To determine the signal-to-noise ratio, regions of interest (ROIs) in the grey and white matter were outlined with Multi Gauge V3.0 software (Fuji) and the optical densities measured as digital light units per square millimetre. The signal-to-noise ratio was obtained by subtracting the nonspecific binding (subcortical white matter region) from the total binding (grey matter regions) and then dividing by the nonspecific binding (i.e. specific binding/nonspecific binding).

High-resolution amyloid-β autoradiography

Emulsion-dipped [^{3}H]AZD2995 labelled tissue sections for microscopic analysis were prepared as described previously [13]. In brief, 10-μm slide-mounted cryo-cut tissue sections were labelled with 1 nM of [^{3}H]AZD2995 and dipped in NTB-2 liquid emulsion (Kodak, Rochester, NY) at 42 °C. The slides were air-dried and exposed for 1–2 weeks in the dark, developed and counterstained with haematoxylin (Histolab, Göteborg, Sweden).

Immunohistochemistry

Frozen tissue sections from APP/PS1 mouse brain and AD cortex were fixed by immersion in 50 % acetone for 1 min and 100 % acetone for 7 min. The immunohistochemistry (IHC) procedure was carried out on an automated stainer (Ventana Discovery XT staining module; Ventana, Illkirch, France) using Ventana kits and the 'no pretreatment' protocol prescribed by the manufacturer. A mix of two different primary antibodies, 4 G8 detecting amyloid-β(27-24) and 6E10 amyloid-β(1-16) (both Signet, Dedham, MA), was manually applied at a dilution of 1:1,000 (1 μg/ml) for detection of total plaque load. For detection of tau pathology, paraffin-embedded paraformaldehyde-fixed (4 %) tissue and a primary anti-human PHF-tau antibody, AT-8 (Innogenetics, Gent, Belgium), at 1 μg/ml were used together with the standard Ventana CCI protocol. A Ventana Omni-ultramap kit was used for detection. Finally, the slides were counterstained with haematoxylin and analysed under the light microscope.

Statistical analysis and software

Data were analysed using GraphPad Prism 4.03 (GraphPad Software, San Diego, CA) or the Excel (Microsoft) based program XL-fit. The results are presented as averages ± SEM (standard error of the mean). Means of K_d, B_{max}, IC_{50} were compared using the *t*-test. Differences were considered significant at $p < 0.05$.

Radiochemistry

[^{3}H]AZD2995 was synthesized by *N*-alkylation of 5-(6-methoxy-1,3-benzoxazol-2-yl)pyridin-2-amine with [^{3}H] methyl iodide in dimethylformamide as solvent and sodium hydride as base as described elsewhere [17]. After purification on a C8 reversed-phase HPLC column (60 % v/v acetonitrile/50 mM ammonium acetate), and subsequent evaporation of eluent, the purified intermediate [^{3}H-*N*-methyl]5-(6-methoxy-1,3-benzoxazol-2-yl)-*N*-methylpyridin-2-amine was dissolved in *N*-methyl-2-pyrrolidone. Demethylation was accomplished by adding sodium thiophenoxide and heating the reaction mixture with microwaves at 250 °C for 30 min. The reaction mixture was purified on a C8 reversed-phase HPLC column (30 % v/v acetonitrile/50 mM ammonium acetate) to yield [^{3}H]AZD2995 with an overall yield of 24 % and a specific activity of 2.5 TBq/mmol. The

radioactive purity was >98 %. The synthesis of [^{3}H]AZD2814 has been described in detail previously [13, 17]. The specific activity of [^{3}H]AZD2184 was 2.9 TBq/mmol with a radioactive purity of >98 %. [^{3}H]PIB (2.9 TBq/mmol, radiochemical purity >99 %) was prepared as described previously [5]. [^{3}H]AZD2995, [^{3}H]AZD2184 and [^{3}H]PIB were stored in absolute ethanol at −18 °C, at radioactivity concentrations of typically 37 MBq/ml.

[^{11}C]AZD2184 and [^{11}C]AZD2995 were synthesized as described in detail elsewhere [12]. After synthesis, the PET ligands [^{11}C]AZD2184 and [^{11}C]AZD2995 were dissolved in a solution of sterile disodium phosphate-buffered saline, pH 7.4, and filtered through a sterile Millipore filter, for direct administration to the subjects.

PET in human subjects

Subjects and study design

Six control subjects and seven patients with mild to moderate AD were included in the study. The focus of the study was to evaluate two novel amyloid-β PET radioligands and not to compare age-matched healthy controls and AD patients. Therefore younger control subjects were recruited to ensure no or negligible amyloid-β load in whom the amount of nonspecific binding could be truly evaluated. The control subjects were considered healthy, with no symptoms of dementia or other neurological disease, after a neuropsychiatric and somatic examination.

All AD patients were recruited from the Memory Clinic, Department of Geriatrics, Karolinska University Hospital Huddinge, Sweden. AD was diagnosed by an experienced geriatrician according to the DSM-IV criteria including a Mini-Mental State Examination (MMSE) score [20] between 16 and 26, brain imaging (MRI or CT) and analysis of biomarkers in cerebrospinal fluid. The study was approved by the Regional Ethics Committee in Stockholm, and was performed in accordance with the Declaration of Helsinki and the International Conference on Harmonization/Good Clinical Practice guidelines. All subjects and caregivers gave written informed consent before enrolment in the study.

All six control subjects and seven AD patients underwent two PET examinations one after intravenous injection of [^{11}C]AZD2995 and the other after injection of [^{11}C]AZD2184. Four of the AD patients underwent a second PET measurement with [^{11}C]AZD2995 as a preliminary investigation of test–retest variability. [^{11}C]AZD2995 was injected as a bolus with a mean ± standard deviation, SD) radioactivity of 410 ± 18 MBq and a specific radioactivity of 620 ± 486 GBq/μmol. [^{11}C]AZD2184 was injected as a bolus with a radioactivity of 399 ± 43 MBq and a specific radioactivity of 486 ± 227 GBq/μmol. There were no significant differences in injected radioactivity or specific radioactivity between the AD patients and the control subjects for either [^{11}C]AZD2995 or [^{11}C]AZD2184 ($p > 0.05$).

MRI and PET experimental procedure

All subjects underwent MRI performed on a 1.5-T GE Medical Systems Signa Excite system at Karolinska University Hospital, Solna. T1-weighted MR images were obtained and used for segmentation of the grey and white matter and for delineation of ROIs. The 3-D MR dataset was reoriented so that the line between the anterior and posterior commissure was in the horizontal plane and the interhemispheric fissure in the sagittal plane. MR images were segmented into grey and white matter and cerebrospinal fluid using the SPM5 segmentation algorithm in MATLAB (Wellcome Trust Centre for Neuroimaging, London, UK; The Mathworks, Natick, MA).

PET data were obtained on a Siemens/CTI high-resolution research tomograph operating in list mode [21]. [^{11}C]AZD2995 and [^{11}C]AZD2184 data were acquired for 93 min and 63 min, respectively, after injection. The list-mode data were binned and reconstructed using iterative reconstruction with point-spread function modelling into a 4-D PET image dataset. For [^{11}C]AZD2995, the dataset contained 38 consecutive time frames (9 × 10 s, 2 × 15 s, 3 × 20 s, 4 × 30 s, 4 × 60 s, 4 × 180 s and 12 × 360 s) with a 3-D array of 256 × 256 × 207 voxels with a size of 1.22 × 1.22 × 1.22 mm [21]. For [^{11}C]AZD2184 the image contained 33 consecutive time frames (9 × 10 s, 2 × 15 s, 3 × 20 s, 4 × 30 s, 4 × 60 s, 4 × 180 s and 7 × 360 s).

Metabolite-corrected arterial input function

The initial part of the arterial plasma input function was derived using an automated blood sampling system during the first 5 min [22]. Discrete samples of about 2.2 ml were then drawn manually at scheduled time points throughout the PET examination (1, 2, 3, 4, 5, 6.5, 7.5, 8.5, 10.5, 13.5, 16.5, 19.5, 24, 30, 36, 42, 48, 54, 60, 66, 72, 78, 84 and 90 min) for measurement of whole-blood and plasma radioactivity concentration. The metabolite analyses were performed using standard methodology as described previously [23], with some minor modifications as described here. Venipuncture (or indwelling catheter) samples of 2.2 ml were collected at fixed time points (4, 10, 20, 30, 40 and 50 min) after radioligand injection. Blood samples were collected into spray-dried K^{+} EDTA tubes and radioactivity was measured in a well counter. Plasma (0.5 ml) was obtained by centrifugation at 2,000 *g* for 1 min. Radioactivity was measured in a well counter, and the plasma was subsequently mixed with 0.7 ml acetonitrile to precipitate plasma proteins. The supernatant (1 ml) obtained after

centrifugation at 2,000 *g* for 1 min was diluted with 1 ml water and the mixture was subsequently analysed using reversed-phase liquid chromatography (Waters μBondapak C18 column 7.8 × 300 mm, 10 μm, with acetonitrile/0.1 M ammonium formate as mobile phase and a flow rate of 6 ml/min). [^{11}C]AZD2995 was analysed using a mobile phase gradient of 40 % to 55 % acetonitrile over 12 min and then a wash-out phase using 80 % acetonitrile.

Regions of interest

Anatomical ROIs were manually delineated on the reoriented 1 × 1 × 1-mm resolution MR images using the Human Brain Atlas [24]. ROIs were delineated as previously defined [25], and included the following regions: anterior cingulate cortex, hippocampus, lateral temporal cortex, parietal cortex, posterior cingulate cortex, prefrontal cortex, pons and putamen. The cerebellum was used as reference region and delineated to include the cortex but avoiding white matter and the vermis. Segmented images of total grey matter white matter and whole brain were created during image processing as described above and used to create the respective ROIs. The segmented grey matter was also used in ROI extraction to only include grey matter voxels in the manually delineated cortical ROIs described above.

Quantitative analysis

[^{11}C]AZD2995 binding was quantified using the linear graphical method proposed by Logan et al. [26]. Using the metabolite-corrected arterial blood curve as input function, six points in the linear part of the Logan plot were fitted to obtain the total distribution volume (V_T) for [^{11}C]AZD2995 (13 to 45 min after injection). In addition, both [^{11}C]AZD2995 and [^{11}C]AZD2184 were evaluated with the reference Logan (refLogan) method using the cerebellum as the reference region. The cerebellum was chosen since it is known to be devoid of substantial amounts of fibrillar amyloid-β [27, 28], and has previously been successfully used as a reference region [14, 29–31]. To obtain the V_T, the

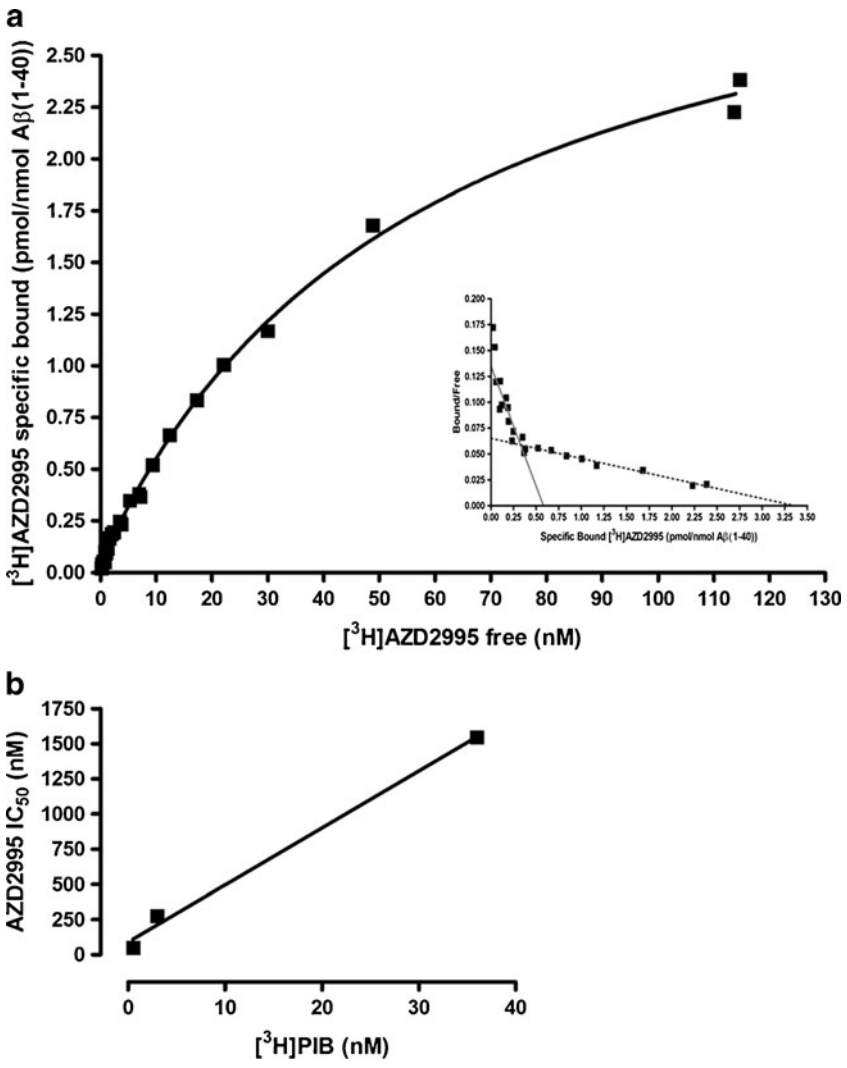

Fig. 1 Saturation binding (**a**) and Scatchard plot (*insert*) showing two distinct binding sites on synthetic Aβ(1-40) fibrils. The high-affinity site (K_d 6.2±0.6 nM) appears at a lower density (B_{max} 0.8±0.1 pmol/nmol) than the low-affinity site (K_d 73.4±7.5 nM; B_{max} 4.3±0.3 pmol/nmol). **b** The IC_{50} values for AZD2995 increased linearly with increasing [^{3}H]PIB concentrations, demonstrating that AZD2995 and PIB bind to the same site in a competitive manner

same number of frames (six) were used in the linear part of the curve for [^{11}C]AZD2995 (13 to 45 min after injection) and [^{11}C]AZD2184 (30 to 60 min). Due to the fast washout of [^{11}C]AZD2995 the low radioactivity in the later part of PET data acquisition resulted in a positive bias due to poor counting statistics. Therefore earlier time frames were used for quantification using the Logan method for [^{11}C]AZD2995 than for [^{11}C]AZD2184.

The distribution volume ratio (DVR) was calculated as the ratio between V_T in the target region divided by that in the reference region, i.e. the cerebellum. Detailed information regarding quantification is planned to be presented elsewhere.

Parametric images for visualization were produced using reference wavelet-aided parametric imaging (refWapi) for noise reduction and parametric calculation performed using the refLogan method in a similar manner to the ROI-based analysis [32]. The outcome measure was the binding potential (BP) calculated as DVR − 1, DVR estimated using the refLogan method performed within refWapi [32].

Statistical analysis and software

Group differences in demographic parameters were analysed in Windows Excel and calculated using a two-tailed *t*-test with unequal variance. Test–retest variability was calculated for each region as the absolute value of the difference between test and retest values divided by the mean of the two measurements. Test–retest variability is reported for selected ROIs as means ± SD across all test–retest subjects in units of percentage. The intraclass correlation coefficients were calculated to characterize measurement reliability [33]. The intraclass correlation coefficient estimates how much of the total variance of the test–retest dataset originates from the measurement error (within-subject variance) in proportion to the intersubject variance (range −1 to 1). Group differences in binding parameters for the corresponding radioligand were calculated using PASW Statistics 18 with independent-samples Mann–Whitney *U* test, and were considered significant at $p < 0.05$. The standardized differences in the group mean estimates between AD patients and control subjects were also calculated. Standardization was based on the pooled standard deviation producing effect size.

Results

Preclinical studies

Binding to amyloid-β fibrils in vitro

Saturation binding studies in vitro with up to 130 nM of [^{3}H]AZD2995 revealed two distinct binding sites on synthetic Aβ(1-40) fibrils as demonstrated by both Scatchard plot analysis (Fig. 1a) and nonlinear regression analysis. The high-affinity site (K_d 6.2±0.6 nM) appears at a lower density (B_{max} 0.8±0.1 pmol/nmol) than the low-affinity site (K_d 73.4±7.5 nM; B_{max} 4.3±0.3 pmol/nmol).

The binding of AZD2995 to amyloid-β fibrils was examined in a competition binding assay in which the displacement of the reference radioligand [^{3}H]PIB from Aβ(1-40) amyloid fibrils was measured at three different concentrations of [^{3}H]PIB (Fig. 1b). AZD2995 bound with high affinity to Aβ(1-40) and was able to successfully displace [^{3}H]PIB binding (Fig. 1b). The pIC_{50} values of AZD2995 increased in a linear fashion with increasing concentrations of [^{3}H]PIB, supporting a competitive interaction between the ligands. The binding of [^{3}H] AZD2995 was reversible with a two-phase dissociation with half-lives ($T_{1/2}$) of 0.2 ± 0.04 min and 8.9 ± 1.2 min. AZD2995 inhibited [^{3}H]PIB (3 nM) binding to synthetic Aβ(1-40) amyloid fibrils with a similar affinity as to Aβ(1-42) amyloid fibrils (pIC_{50} 6.77 ± 0.02; IC_{50} 170.42 nM, pIC_{50} 6.69 ± 0.05; IC_{50} 203.77 nM, respectively).

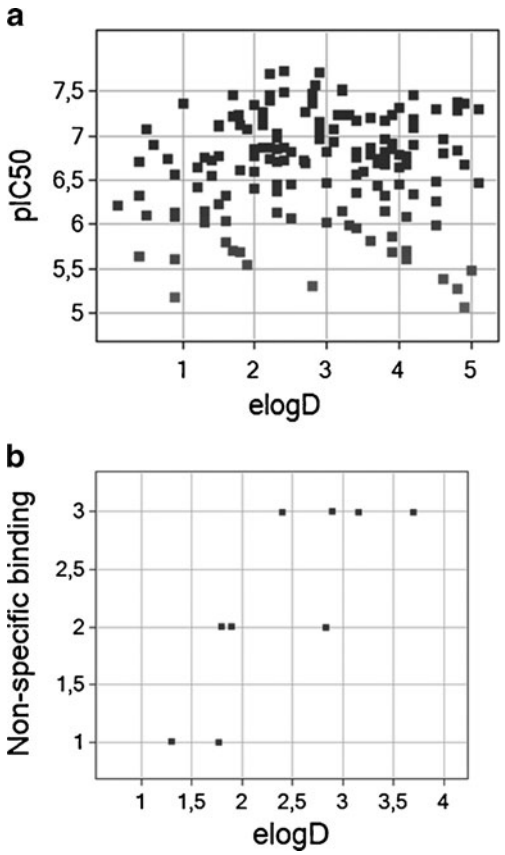

Fig. 2 PET ligand nonspecific binding is correlated well with elogD (**a**), in contrast to ligand affinity towards amyloid which is not correlated with elogD (**b**). Nonspecific binding was determined using autoradiography of the binding of the tritiated ligands to white matter in human brain slices

Nonspecific binding was defined from the autoradiograms of tritiated labelled ligand binding to white matter in human AD brain slices. The analyses comparing reported effective logD (elogD) values [17] with the measured degree of nonspecific binding and amyloid-β fibril affinity revealed that nonspecific binding was correlated with eLogD (Fig. 2a). However, no correlation was found between amyloid-β PET ligand affinity and ligand eLogD (Fig. 2b).

In vitro autoradiography and immunohistochemistry

In vitro binding studies were performed on sections of whole brain from APP/PS1 transgenic mice and dissected cortical tissue sections from AD patients. [^{3}H]AZD2995 selectively labelled amyloid-β plaques in brain sections from APP/PS1 mice and most abundantly in the cortex and hippocampus (data not shown). In vitro binding studies of [^{3}H]PIB, [^{3}H]AZD2184 and [^{3}H]AZD2995 on cortical tissue from AD patients demonstrated binding to amyloid-β deposits in a similar manner (Fig. 3). [^{3}H]AZD2995 and [^{3}H]AZD2184 binding was most abundant in superficial layers of the cortex (grey matter) and more sparse in fibre tracts and in subcortical white matter (Fig. 3). Analysis of amyloid-β binding in post mortem human brain tissue sections, demonstrated that at a radioligand concentration of 3 nmol/l, the ratio between grey matter binding (specific) and white matter binding (nonspecific) was higher for [^{3}H]AZD2995 than for [^{3}H]PIB and [^{3}H]AZD2184 (Fig. 3).

The binding of [^{3}H]AZD2995 and [^{3}H]AZD2184 was examined by comparing autoradiography results with IHC using anti-Aβ selective antibodies in human AD cortical tissue. Microscopic analysis of 7-μm sections of AD brain revealed that the [^{3}H]AZD2995 and [^{3}H]AZD2184 labelling matched the IHC labelling of Aβ (Fig. 4a–c). High-resolution autoradiography revealed selective binding of [^{3}H]AZD2995 and [^{3}H]AZD2184 to dense core amyloid-β plaques as well as diffuse amyloid-β plaques (Fig. 4a–c).

To explore the selectivity of [^{3}H]AZD2995 and [^{3}H]AZD2184 binding to Aβ-fibrils compared to tau deposits (tangles), high-resolution autoradiography of [^{3}H]AZD2995 and [^{3}H]AZD2184 compared to total Aβ IHC (6E10/4 G8) and PHF-tau IHC (AT8) was performed on thin (4-μm) paraffin-embedded adjacent tissue sections. No correlation between tau pathology and [^{3}H]AZD2995 or [^{3}H]AZD2184 binding was observed at 1 nM (Fig. 4d).

PET in human subjects

Before entering human PET studies [^{11}C]AZD2995 was investigated in nonhuman primates to ensure sufficient brain exposure. In nonhuman primates [^{11}C]AZD2995 rapidly entered the brain with an exposure of about 1 % of total injected radioactivity (Supplementary Fig. 1). This observation supported further examination in human subjects. The study was performed according to "The guidelines for planning, conduction, and documenting experimental research" (Dnr 4820/06-600) of Karolinska Institutet as well as the guidelines in

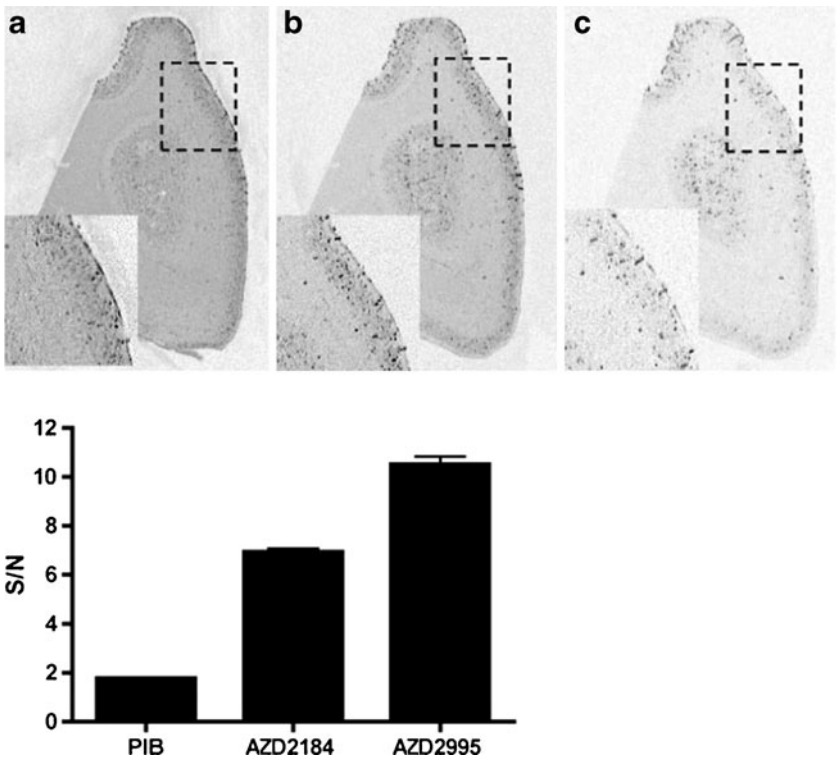

Fig. 3 Autoradiograms of tissue sections from human AD brain incubated with 3 nM of (**a**) [^{3}H]PIB, (**b**) [^{3}H]AZD2184 and (**c**) [^{3}H]AZD2995. Quantification of the signal-to-noise ratios of the three ligands is presented in the bar graph below

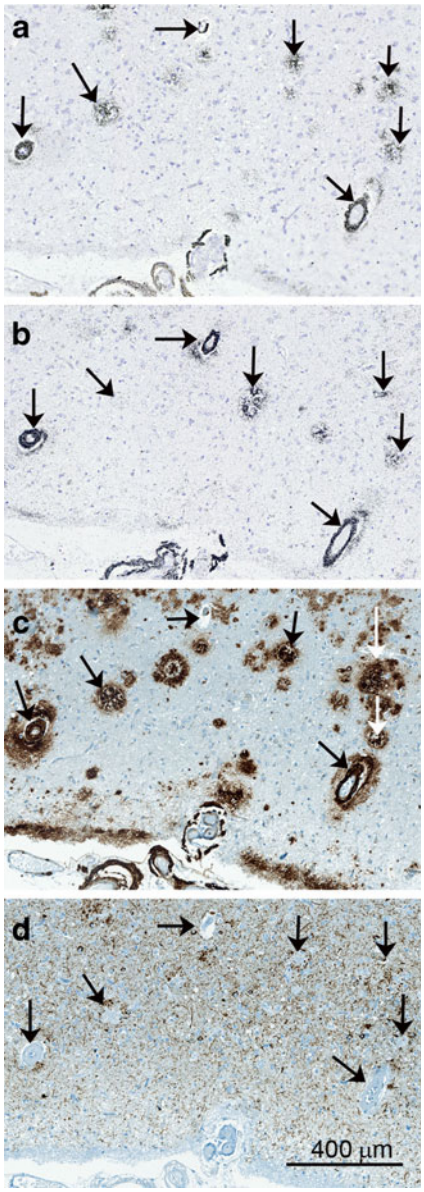

Fig. 4 High-resolution autoradiography imaging of (**a**) 3nM [^{3}H]AZD2995 and (**b**) 3 nM [^{3}H]AZD2184 compared to IHC of (**c**) total amyloid-β plaque load (6E10/4G8) and (**d**) tau pathology (AT-8) in tissue sections from the same AD post mortem brain sample

Principles of Laboratory Animal Care (NIH publication no. 85-23, revised 1985). The study was approved by the Animal Ethics Committee of the Swedish Animal Welfare Agency and was consistent with applicable regulatory requirements and the AstraZeneca policy on Bioethics.

Subjects

Six control subjects (all men) and seven AD patients (six men, one woman) underwent PET examination. Due to technical issues related to data acquisition and storage, data from three control subjects examined in the same week were not usable. The age range of the three remaining control subjects was 24–36 years and the age (mean ± SD) of the AD patients was 68 ± 11 years (range 56 to 81 years). The MMSE score (mean ± SD) was 22 ± 3 in AD patients.

Arterial input function and radioligand metabolism

Blood samples were taken during the [^{11}C]AZD2995 PET examination. Time curves for radioactivity in whole blood and metabolite-corrected plasma were similar across control subjects and AD patients (Fig. 5a). The metabolism of [^{11}C]AZD2995 was very rapid in both AD patients and control subjects. About 50 % of the radioligand was metabolized within 5 min of injection (Fig. 5b). The radioactive metabolites produced were more polar than the parent compound (Fig. 5c).

Time–activity curves

After intravenous injection of [^{11}C]AZD2995 the time–activity curves for total radioactivity in brain increased rapidly reaching a peak after about 1 min when 2.5–3.5 % of radioactivity was in the brain (Fig. 6a). By comparison, the peak for [^{11}C]AZD2184 was reached at the same time as 3.0–3.5 % of radioactivity was seen in the brain (Fig. 6b). Representative time–activity curves for [^{11}C]AZD2995 and [^{11}C]AZD2184 in a control subject and an AD patient are presented in Fig. 7. For both radioligands there was a rapid decline in radioactivity after the initial peak, although the washout was faster for [^{11}C]AZD2995 than for [^{11}C]AZD2184. In AD patients, radioactivity was higher in cortical areas than in the white matter and cerebellum for both radioligands. In the white matter, the radioactivity after injection of [^{11}C]AZD2995 was lower than after injection of [^{11}C]AZD2184. In control subjects, [^{11}C]AZD2995 binding was equal in the grey matter, white matter and cerebellum, while [^{11}C]AZD2184 binding was somewhat higher in the whiter matter.

Quantification

Full kinetic modelling for [^{11}C]AZD2995 and [^{11}C]AZD2184 will be presented elsewhere. Data for [^{11}C]AZD2995 was successfully fitted using the Logan plot with metabolite-corrected arterial input function. The simplified refLogan approach described the data for both [^{11}C]AZD2995 and [^{11}C]AZD2184. Parametric images of BPs for [^{11}C]AZD2995 and [^{11}C]AZD2184 overlaid on respective MR images are presented for representative individuals in Fig. 8. The individual DVRs in the grey matter of control subjects and AD patients are given in Fig. 9. The DVRs estimated for [^{11}C]AZD2995 using the refLogan method were consistent with the DVRs estimated with the Logan method using a

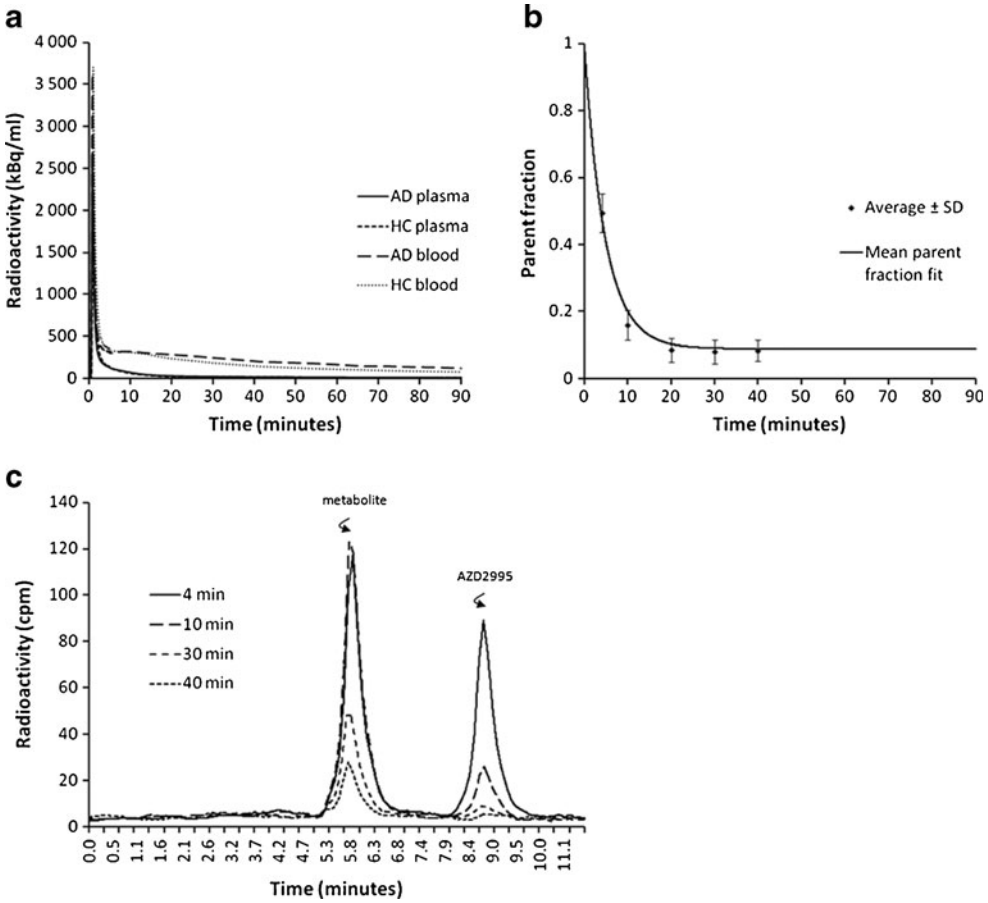

Fig. 5 **a** Group-wise interindividual mean radioactivity concentrations of [^{11}C]AZD2995 in arterial whole blood and metabolite-corrected plasma in AD patients (*AD*, *n*=6) and control subjects (*HC*, *n*=3). **b** Parent fraction of [^{11}C]AZD2995 in relation to time in arterial plasma. **c** Chromatogram showing radioactive parent and metabolites of [^{11}C]AZD2995 at four time points after injection

metabolite-corrected input curve (Supplementary Fig. 2). In all AD patients, the DVRs of the grey matter were lower for [^{11}C]AZD2995 than for [^{11}C]AZD2184.

General observations of regional binding

In control subjects, nonspecific binding was low and homogeneous for both radioligands, and was lower for [^{11}C]AZD2995 (Fig. 8). Specific binding was demonstrated for both radioligands in cortical regions known to have high amounts of amyloid-β plaques including the frontal, parietal and posterior cingulate cortices. In AD patients, the BP values were lower for [^{11}C]AZD2995 than for [^{11}C]AZD2184.

Group differences

The mean DVRs estimated with the refLogan method for [^{11}C]AZD2995 and [^{11}C]AZD2184 are given in Table 1. DVR values for the two radioligands significantly separated control subjects and AD patients (Table 1). The effect sizes were generally smaller for [^{11}C]AZD2995 than for [^{11}C]AZD2184, except for two regions (the lateral temporal

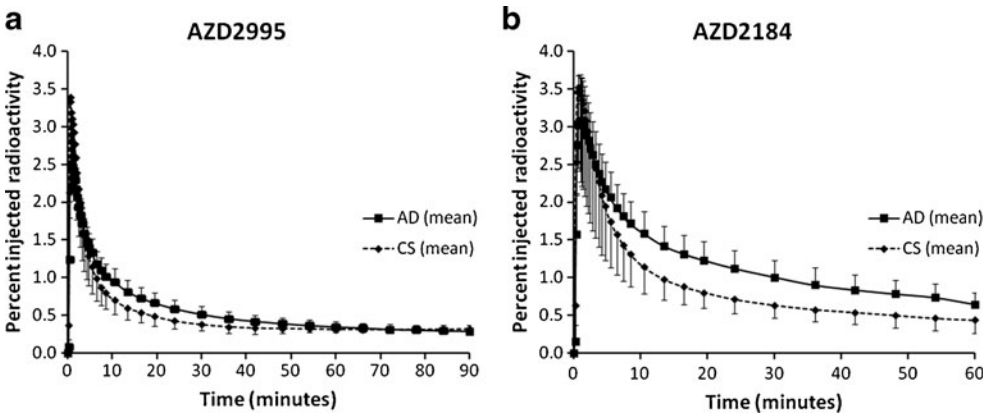

Fig. 6 Percent injected activity (means ± SD) in relation to time for (**a**) [^{11}C]AZD2995 and (**b**) [^{11}C]AZD2184 in AD patients (*AD*) and control subjects (*CS*)

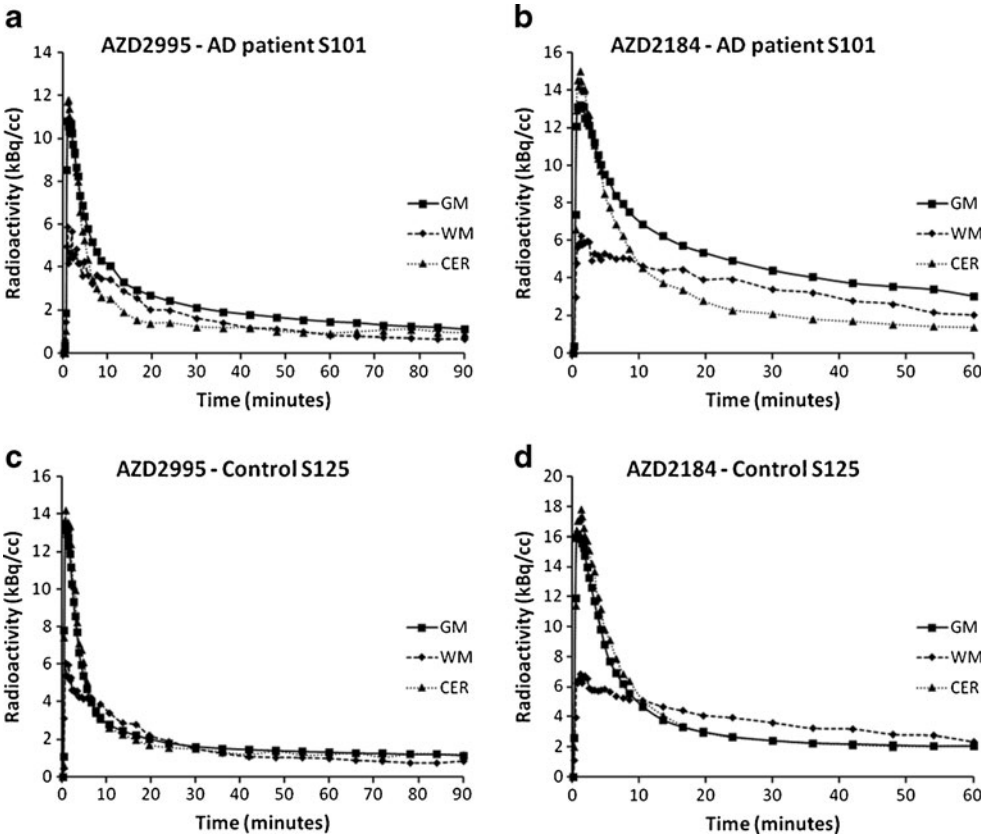

Fig. 7 Representative time–activity curves for [^{11}C]AZD2995 and [^{11}C]AZD2184 in an AD patient (**a**, **b**) and a control subject (**c**, **d**) (*GM* grey matter, *WM* white matter, *CER* cerebellum)

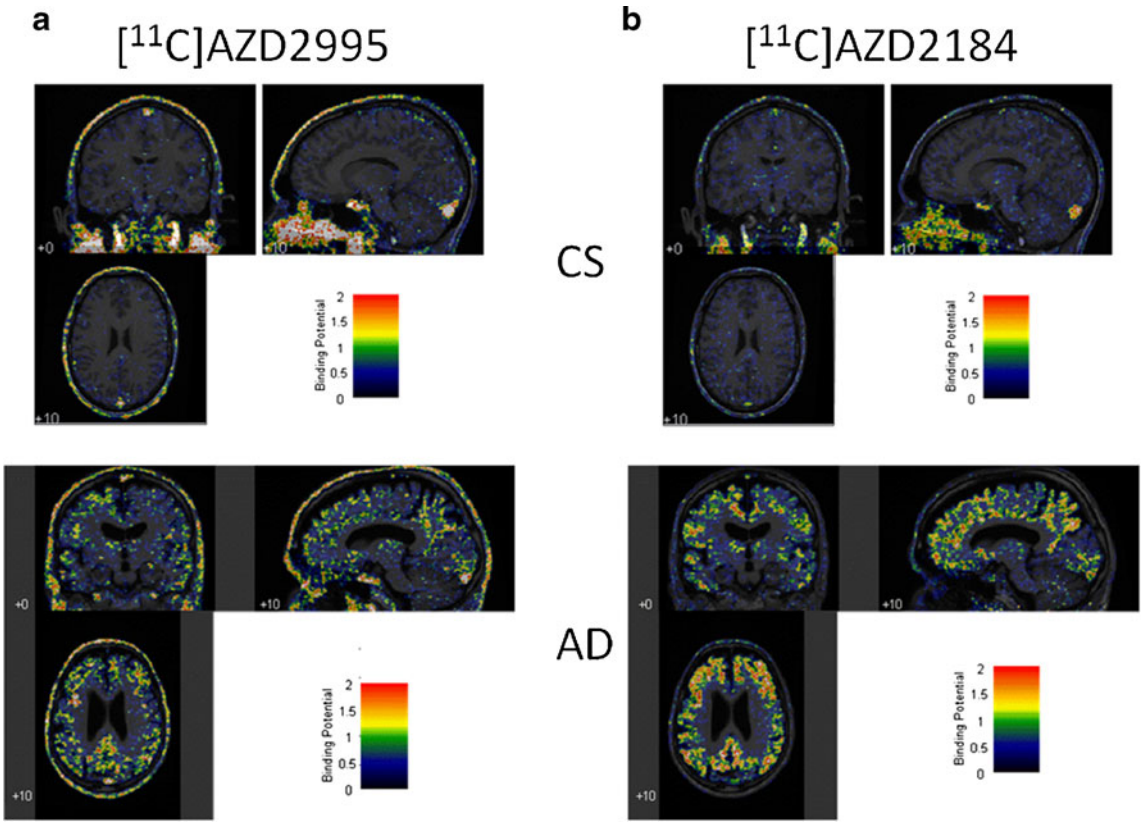

Fig. 8 Parametric images of BPs for [^{11}C]AZD2995 and [^{11}C]AZD2184 overlaid on respective MR images in control subject S124 and AD patient S101

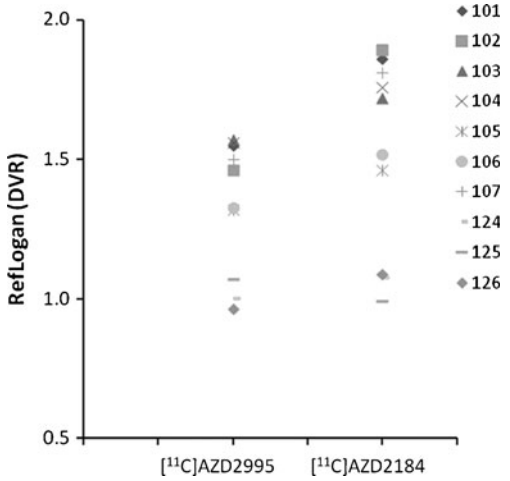

Fig. 9 Individual DVR) values in control subjects (IDs 124–126) and AD patients (IDs 101–107) using [^{11}C]AZD2995 and [^{11}C]AZD2184, respectively

cortex and hippocampus) in which the effect sizes were larger for [^{11}C]AZD2995 than for [^{11}C]AZD2184.

Test–retest variability

Four AD patients (AD4, AD5, AD6 and AD7) underwent a second PET scan with [^{11}C]AZD2995 to estimate the test–retest variability of the radioligand. Regional DVRs estimated using the refLogan method had a test–retest variability ranging from 1.4 % to 4.3 % in the grey matter (Table 2). Intraclass correlation coefficients were generally large, ranging from 0.77 to 0.99.

Discussion

Imaging methodology for accurate measurements of low amounts of amyloid-β would serve as a valuable research tool when studying individuals with AD at a preclinical stage, or when disease progression in relation to disease-modifying treatment is to be followed longitudinally [34]. The currently most widely used amyloid-β radioligand, [^{11}C]PIB, has relatively high nonspecific binding to white matter, which may limit its ability to detect small changes [35]. In the present study, we examined the in vitro and in vivo binding properties of the more recently developed radioligand [^{11}C]AZD2995. This radioligand has low lipophilicity when compared with previously developed radioligands, and the aim was to determine if this physicochemical property translates into advantages for detection of low amounts of amyloid-β.

Binding characteristics

The specificity of AZD2995 binding to amyloid-β was confirmed using binding and competition assays. As is seen with other amyloid-β ligands, one high-affinity and one low-affinity binding site were identified [6, 13]. However, the low-affinity binding site will not significantly contribute to the specific binding component since the radioligands are used in low nanomolar concentrations in PET imaging.

The in vitro binding of [^{3}H]AZD2995 in APP/PS1 transgenic mice and AD post mortem tissue was comparable to that of [^{3}H]AZD2184, being most abundant in areas known to contain large amounts of amyloid-β plaques, including the frontal cortex as shown in the present study, and was distributed in the cortical layers in a pattern similar to that of [^{3}H]PIB [5, 6]. Brain tissue from an ApoE 4/4 carrier was for autoradiography and IHC, and this AD patient was not representative of all AD patients but was appropriate given the aim to compare the binding properties and signal-to-background ratio between the different ligands. Although all three amyloid-β ligands examined in these experiments display a high level of correspondence in their regional

Table 1 DVR values for [^{11}C]AZD2995 and [^{11}C]AZD2184 binding in AD patients and control subjects

Ligand		White matter	Grey matter	Anterior cingulate cortex	Lateral temporal cortex	Parietal cortex	Posterior cingulate cortex	Prefrontal cortex	Hippocampus
[^{11}C]AZD2995	DVR (mean ± SD)								
	AD patients	1.03 ± 0.06	1.47 ± 0.11	1.46 ± 0.14	1.63 ± 0.14	1.68 ± 0.20	1.80 ± 0.18	1.64 ± 0.19	1.20 ± 0.07
	Control subjects	0.75 ± 0.17	1.01 ± 0.05	0.80 ± 0.09	1.01 ± 0.06	0.94 ± 0.08	1.12 ± 0.10	0.94 ± 0.11	1.04 ± 0.04
	Effect size	3.35	5.13	5.44	5.37	4.55	4.49	4.37	2.78
	p value[a]	0.017	0.017	0.017	0.017	0.017	0.017	0.017	0.017
[^{11}C]AZD2184	DVR (mean ± SD)								
	AD patients	1.25 ± 0.05	1.72 ± 0.17	1.97 ± 0.15	1.94 ± 0.22	2.07 ± 0.25	2.10 ± 0.18	2.13 ± 0.23	1.11 ± 0.10
	Control subjects	1.08 ± 0.13	1.05 ± 0.05	0.92 ± 0.02	1.03 ± 0.05	1.04 ± 0.04	1.17 ± 0.02	1.04 ± 0.04	0.95 ± 0.08
	Effect size	2.67	4.89	8.52	5.00	5.26	6.34	5.82	1.73
	p value[a]	0.030	0.017	0.017	0.017	0.017	0.017	0.017	0.030

[a] Significant at $p < 0.05$, calculated using independent-samples Mann–Whitney *U* test.

Table 2 Test–retest variability and intraclass correlation coefficients for [^{11}C]AZD2995

	White matter	Grey matter	Anterior cingulate cortex	Lateral temporal cortex	Parietal cortex	Posterior cingulate cortex	Prefrontal cortex	Hippocampus
Test–retest variability (%)	1.9 ± 1.3	1.1 ± 0.8	4.3 ± 3.0	2.1 ± 0.9	4.2 ± 2.4	1.4 ± 1.0	3.0 ± 1.8	3.9 ± 1.9
Intraclass correlation coefficient	0.90	0.99	0.77	0.97	0.97	0.97	0.98	0.88

selectivity patterns, there were differences regarding the contrast between specific and nonspecific binding (Fig. 3). [^{3}H]AZD2184 demonstrated the highest signal in cortical tissue, but nonspecific binding in the white matter was lowest for [^{3}H]AZD2995. Since AZD2995 has a slightly lower affinity (K_d 6.2 nM) than AZD2184 (K_d 4.9 nM) and PIB (K_d 4.8 nM), this low nonspecific binding may be a major reason for the higher signal-to-background ratio for [^{3}H]AZD2995 than for [^{3}H]AZD2184 and [^{3}H]PIB [13]. Interestingly, the difference in nonspecific binding and background followed the rank order of lipophilicity between the radioligands, with [^{3}H]AZD2995 having the lowest lipophilicity and background, [^{3}H]AZD2184 intermediate and [^{3}H]PIB the highest (Fig. 3). This is in line with what was predicted by the results showing a correlation between lipophilicity and amount of nonspecific binding (Fig. 2a).

The specificity of [^{3}H]AZD2995 binding to amyloid-β was further evaluated by high-resolution imaging of incubated emulsion-dipped tissue sections that were compared with adjacent sections stained for amyloid-β or tau by IHC. [^{3}H]AZD2995 selectively labelled both diffuse plaques and dense core plaques in a similar manner to [^{3}H]PIB [36], [^{3}H]AZD2184 [13] and [^{3}H]AZD4694 [15], while only core plaques were labelled in transgenic mice (Fig. 4). Furthermore, [^{3}H]AZD2995 did not bind tau deposits at low concentrations. Binding to tau will therefore not have an impact on a signal seen with PET using nanomolar concentrations of radioligand.

Initial preclinical characterization suggests that [^{11}C]AZD2184 has the most promising properties for group separation with a higher binding affinity and a strong signal, but radiolabelled AZD2995 might be a more sensitive tool for imaging low levels of amyloid-β in vitro as well as in vivo.

In vivo binding in human subjects

[^{11}C]AZD2995 showed a very low and homogeneously distributed nonspecific binding in control subjects similar to the pattern that has been previously reported for [^{11}C]AZD2184 [14]. There were no obvious differences in regional brain distribution of radioactivity in control subjects after injection of [^{11}C]AZD2995 and [^{11}C]AZD2184, although the latter showed somewhat higher DVR values in most regions. In control subjects, [^{11}C]AZD2995 entered the brain rapidly and the brain exposure was slightly lower than that for [^{11}C]AZD2184 [14]. The lower exposure for [^{11}C]AZD2995 might have been due to the lower nonspecific binding as shown in the preclinical analyses. One limitation of this study was the low number of control subjects due to technical issues in three PET examinations. It is also worth noting that the study was designed to compare the specific binding in AD patients of the two novel amyloid PET radioligands with that in controls devoid of specific binding. This was the reason for inclusion of young healthy controls rather than age-matched control subjects. Further studies are needed to evaluate the sensitivity and specificity of these radioligands in larger age-matched samples.

In AD patients, [^{11}C]AZD2995 as well as [^{11}C]AZD2184 displayed reversible binding and rapid washout. All labelled metabolites of [^{11}C]AZD2995 detected were more polar than the parent as estimated from the elution order on reversed-phase HPLC, which should make them less likely to pass the blood–brain barrier. These observations prompted an initial quantitative analysis using standard quantification methods such as the Logan plot. The regional distribution of [^{11}C]AZD2995 radioactivity in AD patients was similar to that found for other amyloid-β radioligands showing high binding in the parietal, frontal, parietotemporal and posterior cingulate cortices [5, 14, 30]. This observation further supports the preclinical observations of specific binding to amyloid-β plaques.

[^{11}C]AZD2995 showed significant differences in binding between AD patients and healthy controls, although it had a lower effect size than [^{11}C]AZD2184. [^{11}C]AZD2184 may therefore be favoured for further studies aiming at investigating amyloid-β pathology in relation to functional changes and separating subjects with and without amyloid-β pathology. Nevertheless, [^{11}C]AZD2995 showed a greater effect size than [^{11}C]AZD2184 in the hippocampus and the lateral temporal cortex, supporting the notion that this radioligand might be useful for studying areas with small increments in amyloid-β pathology, taking advantage of the low background binding. [^{18}F]FDDNP has so far been the only amyloid ligand for which it has been possible to relate pathological progression and cognitive decline [10, 37], although these findings were not replicated in a study showing no relationship between increased levels of FDDNP and progression from mild cognitive impairment to AD. Recent large studies using [^{11}C]PIB have begun to show patterns

between amyloid deposition and early cognitive changes [38] as well as a markedly greater conversion rate in [^{11}C]PIB-positive patients with mild cognitive impairment than in [^{11}C]PIB-negative patients [39].

Applications

AZD2995 and AZD2184 were developed as amyloid-β ligands with less lipophilicity than PIB in order to achieve improved specific to nonspecific binding ratios. This physicochemical property is the most likely explanation for the improved specific/nonspecific ratio demonstrated in vitro using autoradiography (Fig. 3). This is an advantage in preclinical studies in which higher concentrations are used than for PET in humans. For example, in the present in vitro study concentrations in the range 1–3 nM were used, which are about 60 times higher than the concentration used in PET studies. It should be mentioned that a drawback with ^{11}C ligands compared to ^{18}F ligands is that the positron range of the former is somewhat larger, and this will have a small impact on the resolution. Although the low background binding observed with [^{11}C]AZD2995 could also be important in translational studies using micro-PET in which the injected dose is usually about 20–60 times higher than for PET in humans. The use of a radioligand with very low nonspecific binding could also be an advantage in micro-PET due to the expected larger partial volume effect caused by the very small size of the brain in relation to the resolution of the PET system.

A lot of interest has been shown in the development of ^{18}F-labelled amyloid-β radioligands due their longer half-life. Nevertheless, ^{11}C-labelled radioligands are advantageous in multitracer protocols making it possible to study both amyloid-β load as well as inflammation, receptor levels and glucose metabolism, to mention a few options. Both radioligands showed properties indicating their potential value as research tools. [^{11}C]AZD2995 showed better separation in regions such as the hippocampus which are known to have lower amyloid-β pathology but are still involved in functional deterioration, and [^{11}C]AZD2184 showed higher specific binding and good separation between AD patients and control subjects. The potential usefulness of [^{11}C]AZD2995 in translational and clinical research is further supported by the low test–retest variability, even lower than that shown by [^{11}C]PIB [29, 40].

Conclusion

[^{11}C]AZD2995 as well as [^{11}C]AZD2184 have low lipophilicity which results in very low nonspecific binding and high signal-to-background ratio in AD brain tissue. The low nonspecific binding was further established in PET in humans which highlighted the ability of [^{11}C]AZD2995 to depict amyloid-β pathology in areas with only a slight increase. In small-animal PET the high contrast seen with [^{11}C]AZD2995 could be of importance in allowing the study of small brain structures. [^{11}C]AZD2995 could therefore be a valuable tool in studies focusing on early prodromal stages of AD, in longitudinal studies, or in micro-PET.

Acknowledgments Financial support from the Swedish Research Council (project 09114) and the KI Foundation is gratefully acknowledged. The authors thank the staff of the Karolinska Institutet PET Centre for excellent technical assistance.

Conflicts of interest A.F., M.E., Y.F.-L., J.A., K.V. and CH have no conflicts of interest. Z.C., M.S., P.J. and L.F. are employees and shareholders of AstraZeneca Pharmaceuticals. At the time of the study A.J., F.J., B.-M.S., J.S., P.J. and S.S. were employees of AstraZeneca Pharmaceuticals.

References

1. Mirra SS, Heyman A, McKeel D, Sumi SM, Crain BJ, Brownlee LM, et al. The Consortium to Establish a Registry for Alzheimer's Disease (CERAD). Part II. Standardization of the neuropathologic assessment of Alzheimer's disease. Neurology. 1991;41:479–86.
2. Hyman BT, Trojanowski JQ. Consensus recommendations for the postmortem diagnosis of Alzheimer disease from the National Institute on Aging and the Reagan Institute Working Group on diagnostic criteria for the neuropathological assessment of Alzheimer disease. J Neuropathol Exp Neurol. 1997;56:1095–7.
3. Klunk W, Wang Y, Huang G, Debnath M, Holt D, Shao L, et al. The binding of 2-(4′-methylaminophenyl)benzothiazole to postmortem brain homogenates is dominated by the amyloid component. J Neurosci. 2003;23:2086–92.
4. Klunk W, Wang Y, Huang G, Debnath M, Holt D, Mathis C. Uncharged thioflavin-T derivatives bind to amyloid-beta protein with high affinity and readily enter the brain. Life Sci. 2001;69:1471–84.
5. Klunk W, Engler H, Nordberg A, Wang Y, Blomqvist G, Holt D, et al. Imaging brain amyloid in Alzheimer's disease with Pittsburgh Compound-B. Ann Neurol. 2004;55:306–19. doi:10.1002/ana.20009.
6. Klunk W, Lopresti B, Ikonomovic M, Lefterov I, Koldamova R, Abrahamson E, et al. Binding of the positron emission tomography tracer Pittsburgh compound-B reflects the amount of amyloid-beta in Alzheimer's disease brain but not in transgenic mouse brain. J Neurosci. 2005;25:10598–606. doi:10.1523/JNEUROSCI.2990-05.2005.
7. Maeda J, Ji B, Irie T, Tomiyama T, Maruyama M, Okauchi T, et al. Longitudinal, quantitative assessment of amyloid, neuroinflammation, and anti-amyloid treatment in a living mouse model of Alzheimer's disease enabled by positron emission tomography. J Neurosci. 2007;27:10957–68. doi:10.1523/JNEUROSCI.0673-07.2007.
8. Small G, Kepe V, Ercoli L, Siddarth P, Bookheimer S, Miller K, et al. PET of brain amyloid and tau in mild cognitive impairment. N Engl J Med. 2006;355:2652–63. doi:10.1056/NEJMoa054625.
9. Tolboom N, Yaqub M, van der Flier W, Boellaard R, Luurtsema G, Windhorst A, et al. Detection of Alzheimer pathology in vivo using both 11C-PIB and 18F-FDDNP PET. J Nucl Med. 2009;50:191–7. doi:10.2967/jnumed.108.056499.

10. Small GW, Siddarth P, Kepe V, Ercoli LM, Burggren AC, Bookheimer SY, et al. Prediction of cognitive decline by positron emission tomography of brain amyloid and tau. Arch Neurol. 2012;69:215–22. doi:10.1001/archneurol.2011.559.
11. Ossenkoppele R, Tolboom N, Foster-Dingley JC, Adriaanse SF, Boellaard R, Yaqub M, et al. Longitudinal imaging of Alzheimer pathology using [11C]PIB, [18F]FDDNP and [18F]FDG PET. Eur J Nucl Med Mol Imaging. 2012;39:990–1000. doi:10.1007/s00259-012-2102-3.
12. Andersson JD, Varnäs K, Cselényi Z, Gulyás B, Wensbo D, Finnema SJ, et al. Radiosynthesis of the candidate beta-amyloid radioligand [(11)C]AZD2184: Positron emission tomography examination and metabolite analysis in cynomolgus monkeys. Synapse. 2010;64:733–41. doi:10.1002/syn.20782.
13. Johnson A, Jeppsson F, Sandell J, Wensbo D, Neelissen J, Juréus A, et al. AZD2184: a radioligand for sensitive detection of beta-amyloid deposits. J Neurochem. 2009;108:1177–86. doi:10.1111/j.1471-4159.2008.05861.x.
14. Nyberg S, Jönhagen M, Cselényi Z, Halldin C, Julin P, Olsson H, et al. Detection of amyloid in Alzheimer's disease with positron emission tomography using [11C]AZD2184. Eur J Nucl Med Mol Imaging. 2009;36:1859–63. doi:10.1007/s00259-009-1182-1.
15. Juréus A, Swahn BM, Sandell J, Jeppsson F, Johnson AE, Johnström P, et al. Characterization of AZD4694, a novel fluorinated Abeta plaque neuroimaging PET radioligand. J Neurochem. 2010;114:784–94. doi:10.1111/j.1471-4159.2010.06812.x.
16. Cselényi Z, Jönhagen ME, Forsberg A, Halldin C, Julin P, Schou M, et al. Clinical validation of 18F-AZD4694, an amyloid-β-specific PET radioligand. J Nucl Med. 2012;53:415–24. doi:10.2967/jnumed.111.094029.
17. Swahn BM, Wensbo D, Sandell J, Sohn D, Slivo C, Pyring D, et al. Synthesis and evaluation of 2-pyridylbenzothiazole, 2-pyridylbenzoxazole and 2-pyridylbenzofuran derivatives as 11C-PET imaging agents for beta-amyloid plaques. Bioorg Med Chem Lett. 2010;20:1976–80. doi:10.1016/j.bmcl.2010.01.105.
18. Hsiao K, Chapman P, Nilsen S, Eckman C, Harigaya Y, Younkin S, et al. Correlative memory deficits, Abeta elevation, and amyloid plaques in transgenic mice. Science. 1996;274:99–102.
19. Duff K, Eckman C, Zehr C, Yu X, Prada CM, Perez-tur J, et al. Increased amyloid-beta42(43) in brains of mice expressing mutant presenilin 1. Nature. 1996;383:710–3. doi:10.1038/383710a0.
20. Folstein MF, Folstein SE, McHugh PR. "Mini-mental state". A practical method for grading the cognitive state of patients for the clinician. J Psychiatr Res. 1975;12:189–98.
21. Varrone A, Sjöholm N, Eriksson L, Gulyás B, Halldin C, Farde L. Advancement in PET quantification using 3D-OP-OSEM point spread function reconstruction with the HRRT. Eur J Nucl Med Mol Imaging. 2009;36:1639–50. doi:10.1007/s00259-009-1156-3.
22. Farde L, Eriksson L, Blomquist G, Halldin C. Kinetic analysis of central [11C]raclopride binding to D2-dopamine receptors studied by PET – a comparison to the equilibrium analysis. J Cereb Blood Flow Metab. 1989;9:696–708.
23. Halldin C, Farde L, Högberg T, Mohell N, Hall H, Suhara T, et al. Carbon-11-FLB 457: a radioligand for extrastriatal D2 dopamine receptors. J Nucl Med. 1995;36:1275–81.
24. Roland PE, Zilles K. Brain atlases – a new research tool. Trends Neurosci. 1994;17:458–67.
25. Svarer C, Madsen K, Hasselbalch SG, Pinborg LH, Haugbøl S, Frøkjaer VG, et al. MR-based automatic delineation of volumes of interest in human brain PET images using probability maps. Neuroimage. 2005;24:969–79. doi:10.1016/j.neuroimage.2004.10.017.
26. Logan J, Fowler JS, Volkow ND, Wolf AP, Dewey SL, Schlyer DJ, et al. Graphical analysis of reversible radioligand binding from time-activity measurements applied to [N-11C-methyl]-(-)-cocaine PET studies in human subjects. J Cereb Blood Flow Metab. 1990;10:740–7.
27. Yamaguchi H, Hirai S, Morimatsu M, Shoji M, Nakazato Y. Diffuse type of senile plaques in the cerebellum of Alzheimer-type dementia demonstrated by beta protein immunostain. Acta Neuropathol. 1989;77:314–9.
28. Svedberg M, Hall H, Hellström-Lindahl E, Estrada S, Guan Z, Nordberg A, et al. [(11)C]PIB-amyloid binding and levels of Abeta40 and Abeta42 in postmortem brain tissue from Alzheimer patients. Neurochem Int. 2009;54:347–57. doi:10.1016/j.neuint.2008.12.016.
29. Price J, Klunk W, Lopresti B, Lu X, Hoge J, Ziolko S, et al. Kinetic modeling of amyloid binding in humans using PET imaging and Pittsburgh Compound-B. J Cereb Blood Flow Metab. 2005;25:1528–47. doi:10.1038/sj.jcbfm.9600146.
30. Rowe C, Ackerman U, Browne W, Mulligan R, Pike K, O'Keefe G, et al. Imaging of amyloid beta in Alzheimer's disease with 18F-BAY94-9172, a novel PET tracer: proof of mechanism. Lancet Neurol. 2008;7:129–35. doi:10.1016/S1474-4422(08)70001-2.
31. Wong DF, Rosenberg PB, Zhou Y, Kumar A, Raymont V, Ravert HT, et al. In vivo imaging of amyloid deposition in Alzheimer disease using the radioligand 18F-AV-45 (florbetapir [corrected] F 18). J Nucl Med. 2010;51:913–20. doi:10.2967/jnumed.109.069088.
32. Cselényi Z, Olsson H, Farde L, Gulyás B. Wavelet-aided parametric mapping of cerebral dopamine D2 receptors using the high affinity PET radioligand [11C]FLB 457. Neuroimage. 2002;17:47–60.
33. Shrout PE, Fleiss JL. Intraclass correlations: uses in assessing rater reliability. Psychol Bull. 1979;86:420–8.
34. Hampel H, Wilcock G, Andrieu S, Aisen P, Blennow K, Broich K, et al. Biomarkers for Alzheimer's disease therapeutic trials. Prog Neurobiol. 2011;95:579–93. doi:10.1016/j.pneurobio.2010.11.005.
35. Lansbury PT, Lashuel HA. A century-old debate on protein aggregation and neurodegeneration enters the clinic. Nature. 2006;443:774–9. doi:10.1038/nature05290.
36. Lockhart A, Lamb J, Osredkar T, Sue L, Joyce J, Ye L, et al. PIB is a non-specific imaging marker of amyloid-beta (Abeta) peptide-related cerebral amyloidosis. Brain. 2007;130:2607–15. doi:10.1093/brain/awm191.
37. Protas HD, Kepe V, Hayashi KM, Klunder AD, Braskie MN, Ercoli L, et al. Prediction of cognitive decline based on hemispheric cortical surface maps of FDDNP PET. Neuroimage. 2012;61:749–60. doi:10.1016/j.neuroimage.2012.02.056.
38. Kantarci K, Lowe V, Przybelski SA, Weigand SD, Senjem ML, Ivnik RJ, et al. APOE modifies the association between Aβ load and cognition in cognitively normal older adults. Neurology. 2012;78:232–40. doi:10.1212/WNL.0b013e31824365ab.
39. Nordberg A, Carter SF, Rinne J, Drzezga A, Brooks DJ, Vandenberghe R, et al. A European multicentre PET study of fibrillar amyloid in Alzheimer's disease. Eur J Nucl Med Mol Imaging. 2013;40:104–14. doi:10.1007/s00259-012-2237-2.
40. Engler H, Forsberg A, Almkvist O, Blomquist G, Larsson E, Savitcheva I, et al. Two-year follow-up of amyloid deposition in patients with Alzheimer's disease. Brain. 2006;129:2856–66. doi:10.1093/brain/awl178.